Ascorbate efflux as a new strategy for iron reduction and transport in plants.

Louis Grillet, Laurent Ouerdane, Paulina Flis, Minh Thi Thanh Hoang, M.-P. Isaure, Ryszard Lobinski, Catherine Curie, Stéphane Mari

THE JOURNAL OF BIOLOGICAL CHEMISTRY VOL. 289, NO. 5, pp. 2515–2525, January 31, 2014

Ascorbate Efflux as a New Strategy for Iron Reduction and Transport in Plants*

Received for publication, August 30, 2013, and in revised form, December 16, 2013 Published, JBC Papers in Press, December 17, 2013, DOI 10.1074/jbc.M113.514828

Louis Grillet[‡1,2], Laurent Ouerdane[§1], Paulina Flis[§], Minh Thi Thanh Hoang[‡], Marie-Pierre Isaure[§], Ryszard Lobinski[§], Catherine Curie[‡], and Stéphane Mari[‡3]

From the [‡]Laboratoire de Biochimie et Physiologie Moléculaire des Plantes, Institut de Biologie Intégrative des Plantes, Centre National de la Recherche Scientifique (UMR5004), Institut National de la Recherche Agronomique, Université Montpellier II, Ecole Nationale Supérieure d'Agronomie, 34060 Montpellier Cedex 2, France and the [§]Laboratoire de Chimie Analytique Bio-Inorganique et Environnement, Institut Pluridisciplinaire de Recherche sur l'Environnement et les Matériaux, Centre National de la Recherche Scientifique (UMR5254), Université de Pau et des Pays de l'Adour, 64063 Pau Cedex 9, France

Background: Iron long distance transport in plants is underdocumented.
Results: Iron is delivered to embryos as ferric complexes with citrate/malate. An ascorbate-mediated reduction step is further required to acquire iron.
Conclusion: Ascorbate plays a key role for the chemical reduction and transport of Fe^{2+}.
Significance: The identification of iron ligands and the transport process is crucial to further understand how iron is distributed within the plant.

Iron (Fe) is essential for virtually all living organisms. The identification of the chemical forms of iron (the speciation) circulating in and between cells is crucial to further understand the mechanisms of iron delivery to its final targets. Here we analyzed how iron is transported to the seeds by the chemical identification of iron complexes that are delivered to embryos, followed by the biochemical characterization of the transport of these complexes by the embryo, using the pea (*Pisum sativum*) as a model species. We have found that iron circulates as ferric complexes with citrate and malate ($Fe(III)_3Cit_2Mal_2$, $Fe(III)_3Cit_3Mal_1$, $Fe(III)Cit_2$). Because dicotyledonous plants only transport ferrous iron, we checked whether embryos were capable of reducing iron of these complexes. Indeed, embryos did express a constitutively high ferric reduction activity. Surprisingly, iron(III) reduction is not catalyzed by the expected membrane-bound ferric reductase. Instead, embryos efflux high amounts of ascorbate that chemically reduce iron(III) from citrate-malate complexes. *In vitro* transport experiments on isolated embryos using radiolabeled ^{55}Fe demonstrated that this ascorbate-mediated reduction is an obligatory step for the uptake of iron(II). Moreover, the ascorbate efflux activity was also measured in *Arabidopsis* embryos, suggesting that this new iron transport system may be generic to dicotyledonous plants. Finally, in embryos of the ascorbate-deficient mutants *vtc2-4*, *vtc5-1*, and *vtc5-2*, the reducing activity and the iron concentration were reduced significantly. Taken together, our results identified a new iron transport mechanism in plants that could play a major role to control iron loading in seeds.

Iron is an essential micronutrient for plants. It is used as an enzymatic cofactor in a wide range of metabolic processes, such as photosynthetic and respiratory electron transfer reactions, reduction of nitrate and sulfate, synthesis of fatty acids, and branched amino acids. Iron was selected on the basis of the redox capacity of the Fe^{2+}/Fe^{3+} couple that can exchange one electron. This chemical property is also responsible for the potential toxicity of iron in excess conditions because ferrous ions can promote, in the presence of oxygen, the generation of reactive oxygen species and oxidative stress. Plants, as sessile organisms, must maintain a strict iron balance to cope with deficiency or excess conditions. At the whole plant level, this is achieved by the fine regulation of root absorption, allocation to the aerial parts, storage, and remobilization.

Although very abundant in soils, iron is often poorly available to plants because the main iron form, iron(III), has a very limited solubility and is prone to precipitate in alkaline and neutral conditions. Therefore, plants have developed strategies to efficiently acquire iron. In roots of dicotyledonous species, such as the model plant *Arabidopsis thaliana*, the uptake of iron requires the acidification of the rhizosphere by the proton pumping activity of the ATPase AHA2 (1) to release Fe^{3+} bound to humic substances and mineral phases, the reduction of ferric ions by the ferric chelate reductase encoded by *FRO2* (2),[4] and the subsequent uptake of Fe^{2+} by the metal transporter IRT1 (3–6).

* This work was supported by the Centre National de la Recherche Scientifique, by l'Institut National de la Recherche Agronomique, and by Agence Nationale pour la Recherche Grants 23643 (CIDS) and 07-3-18-8-87 (DISTRIMET).
[1] Both authors contributed equally to this work.
[2] Supported by a Ph.D. fellowship from the Plant Biology Department of the Institut National de la Recherche Agronomique.
[3] To whom correspondence should be addressed: Laboratoire de Biochimie et Physiologie Moléculaire des Plantes, Institut de Biologie Intégrative des Plantes, Centre National de la Recherche Scientifique (UMR5004), Institut National de la Recherche Agronomique, Université Montpellier II, Ecole Nationale Supérieure d'Agronomie, 34060 Montpellier Cedex 2, France. Tel.: 33-4-99-61-25-72; Fax: 33-4-67-52-57-37; E-mail: mari@supagro.inra.fr.

[4] The abbreviations used are: FRO, ferric reductase oxidase; NA, nicotianamine; YSL, yellow stripe 1-like; ESL, embryo sac liquid; XANES, x-ray absorption near edge structure; ESI, electrospray ionization; BPDS, bathophenanthroline disulfonate; AOX, ascorbate oxidase; Cit, citrate; Mal, malate; VTC, vitamin C; HILIC, hydrophilic interaction liquid chromatography; ICP, inductively coupled plasma.

When in root cells, iron atoms must reach the vascular system and enter the xylem vessels to be transported to the aerial parts. Xylem loading is controlled, at least in part, by the FRD3 protein that belongs to the multidrug and toxic compound extrusion family of transporters (7). FRD3 is a citrate effluxer expressed in the root pericycle, whose activity is required to solubilize iron in the xylem sap (8), where citrate was identified as the main iron ligand (9), hence promoting iron movement into the xylem. In leaves, unloading of iron from xylem vessels and distribution in the surrounding cells also requires FRD3 (10). Likewise, the oligopeptide transporter OPT3 (11) contributes to iron movement in leaves, but its substrate, whether it is an iron ligand or an iron complex, is still unknown (11). To date, the number of organic molecules shown to form complexes with iron *in vivo* is extremely limited. Beside citrate, most of the information concerns nicotianamine (NA). This aminopropyl polymer, enzymatically synthesized from *S*-adenosylmethionine, has a high affinity for iron, copper, and zinc. Several studies have shown that the chemical properties and the binding capacity of NA make it an ideal ligand for iron in neutral, cytosolic conditions, whereas in acidic, apoplastic conditions, citrate will prevail (12, 13). *In planta*, NA is involved in the root-to-shoot transport of copper in tomato (14) and nickel and zinc in the hyperaccumulator species *Thlaspi caerulescens* (15, 16). For nickel, the formation of a complex between nicotianamine and nickel in xylem exudates has been demonstrated unambiguously by the coupling of chromatography and mass spectrometry (15, 18).

In *A. thaliana*, several genetic approaches have allowed to pinpoint the role of NA in the transport of iron. The impairment of NA production, through the inactivation of all four NA synthase-encoding genes, provokes the expected phenotype of interveinal chlorosis described for the NA-free tomato mutant *chloronerva* and, more interestingly, a reduced accumulation of iron in seeds (19). Such an impact on seeds has also been reported in mutants of the yellow stripe 1-like (YSL) family of NA-metal transporters. The mutation in *AtYSL1* results in decreased iron and NA accumulation in seeds (20), most likely caused by a reduced remobilization from old leaves, as shown for the *Arabidopsis ysl1ysl3* double mutant (20, 21). Taken together, these results indicate that disturbing the long distance transport of iron has a major impact on the process of seed loading (reviewed in Ref. 22). Seeds represent the most important sink for plants and the end point of long distance circulation of nutrients (23, 24). Virtually nothing is known about the transport pathway that leads to iron loading in the seeds and on the chemical forms (*i.e.* the speciation) of iron during this process. The speciation of a metal ion in a specific biological compartment is crucial information to further understand how the metal is kept soluble, transported across membranes, and delivered to its final target.

In this work, the pea (*Pisum sativum*) was chosen as a biochemical model to study the mechanisms of iron acquisition by the embryo. Grain legumes are particularly suited to study the processes of transport in seeds. One specific feature of these seeds is that the bulk flow of nutrients delivered by the seed coat accumulates in large amounts, forming a liquid endosperm also termed embryo sac liquid (ESL). This particular liquid is of high biological importance because it serves directly to feed the embryo (25). We first analyzed the speciation of iron in isolated ESL using chromatography coupled to mass spectrometry and synchrotron radiation x-ray absorption spectroscopy. This information was crucial to further characterize the transport machinery that is expressed at the embryo surface to acquire iron from maternal tissues.

EXPERIMENTAL PROCEDURES

Plant Material

Pea (*P. sativum* L., Dippes Gelbe Viktoria, DGV, cultivar) and *A. thaliana* (cultivar Col-0) were used in this study. Plants were grown in a greenhouse at 23 °C, in 3-liter pots containing 0.5 liter of quartz sand and 2.25 liters of Humin substrate N2 Neuhaus (Klasmann-Deilmann, Geeste, Germany) irrigated with tap water. Plants used for pea root ferric-chelate reductase measurement were grown hydroponically for 15 days in a climate chamber at 20 °C, 70% hygrometry, 16 h light/8 h dark, and 250 μmol photons/m^2/s of photosynthetically active radiation. The nutrient solution contained 1.25 mM KNO_3, 1.5 mM $Ca(NO_3)2$, 0.75 mM $MgSO_4$, 0.5 mM KH_2PO_4, 25 μM H_3Bo_3, 2 μM $MnSO_4$, 2 μM $ZnSO_4$, $CuSO_4$, Na_2MoO_4, and 0.1 μM $NiCl_2$, buffered pH 5 with 1 mM 2-(*N*-morpholino)ethanesulfonic acid. For iron-deficient plants, no iron was added to this solution, and iron-sufficient plants were fed with 50 μM iron(III)-EDTA.

For *Arabidopsis* root ferric chelate reductase experiments, plants were cultivated *in vitro* on half strength Murashige/Skoog medium supplemented with 50 μM iron-EDTA. After 10 days, plantlets were transferred in an MS medium without iron and containing 30 μM FerroZine for 3 days.

Liquid Endosperm Sampling

Developing pods were dissected with a surgical blade. Two holes were pierced into each seed using a glass capillary tube. The liquid endosperm was then extracted quickly with another glass capillary using a peristaltic pump and blown gently at the bottom of an Eppendorf tube kept on ice. Pumping was carried out carefully to avoid bubbling. Samples were then maintained frozen in liquid nitrogen and kept at −80 °C until further analysis.

Iron Speciation by X-ray Absorption Spectroscopy

Iron K-edge x-ray absorption near edge structure (XANES) measurements were performed on LUCIA Beamline at Soleil Synchrotron, Gif sur Yvette, France, operating at 2.75 GeV (26). The x-ray beam was monochromatized using a Si(111) two-crystal monochromator, and spectra were collected in fluorescence mode using a Bruker Silicon Drift diode and a non-focused beam. All measurements were done in a vacuum and in cryo conditions with a He cryostat providing a temperature of 110 K on the sample holder. A few drops of glycerol were added to liquid references to minimize the formation of ice crystals. No glycerol was added to the ESL because it already contains high concentrations of sugars. Energy was calibrated with metallic iron. The XANES spectra were corrected from background absorption by subtracting a linear function before the

edge and normalizing using a linear or to-degree polynome. A fingerprint approach was then used to simulate the experimental spectra by a linear combination of iron reference compound spectra. The quality of the fits was estimated by the normalized sum-squares residuals $NSS = \Sigma\ (\text{Xanes}_{\text{experimental}} - \text{Xanes}_{\text{fit}})^2 / \Sigma\ (\text{Xanes}_{\text{experimental}})^2 \times 100$ in the 7090-7380 eV range. The iron valence was also estimated by the examination of the pre-edge structure (27).

Iron reference compounds were prepared for comparison with ESL samples. Aqueous 50 mM iron(II) and iron(III) was prepared by dissolving $FeCl_2$ and $FeCl_3$ in deionized water at pH 2. Iron(II) preparation was performed in an argon atmosphere just before analysis to prevent iron oxidation. 25 mM iron(III)-citrate, iron(II)-citrate, and iron(III)-malate were prepared with metal/ligand (M/L) = 1/10 at pH 5.6 and 5.2, respectively. On the basis of the Visual MINTEQ software for chemical speciation (28), under these conditions, more than 99% of iron is found as organic complexes. Iron(III)-histidine was synthesized at pH 7.2 with a 1/10 ratio and a total iron concentration of 3.1 mM.

Iron Complexes by Chemical Analysis

Instrumentation—Chromatographic separations were performed using a model 1100 HPLC pump (Agilent, Wilmington, DE) as the delivery system. The HILIC column was a TSK gel amide 80 (250 × 1 mm inner diameter) (Tosoh Bioscience, Germany). All connections were made of fused silica/PEEK tubing (0.050 mm inner diameter). The ICP MS instrument was Agilent 7500cs (Agilent Technologies, Japan) equipped with a collision cell with hydrogen as collision gas. The interface between HPLC and the Agilent 7500cs consisted of a glass Cinnabar cyclonic spray chamber (Glass Expansion, Australia), a Micromist U-series nebulizer (Glass Expansion), a 1-mm inner diameter quartz torch (Agilent Technologies), and a set of platinum cones (Agilent Technologies). The ESI MS instrument was an LTQ Orbitrap Velos mass spectrometer (Thermo Scientific, San Jose, CA).

LC MS Experimental Conditions—The mobile phase was 5 mmol/liter ammonium acetate buffer (pH adjusted to 5.5 by addition of acetic acid) (A) and acetonitrile (B). Analytical reagent-grade chemicals were used for buffer preparation and were purchased from Sigma-Aldrich (Saint Quentin, Fallavier, France). Water (18.2 MΩ/cm) was obtained with a Milli-Q system (Millipore, Bedford, MA). The optimized HILIC gradient started with 10% of A and was increasing to 50% of A during 25 min. The samples (diluted in acetonitrile 1/2, v/v, and 7-μl injection) were eluted at a flow rate of 50 μl/min. Iron-containing species were detected by direct online coupling of the HILIC column to the ICP MS instrument (following signals for ^{54}Fe and ^{56}Fe isotopes) and to the ESI MS instrument. The settings and parameters of ICP MS and ESI MS instruments were optimized daily for highest intensities and lowest interferences using a built-in software procedure (ICP) and a standard mixture recommended by the constructor (ESI). ES MS spectra were acquired with a maximum injection time of 400 ms in the range of 230–1000 mass units. The electrospray voltage was set at 3 kV in positive ion mode and −3 kV in negative ion mode. The ions were fragmented by higher-energy collisional dissociation at various energy levels.

Ferric Reduction Assays—Ferric chelate reductase activity was estimated as the quantity of iron-bathophenanthroline disulfonate (BPDS) complexes formed in the assay solution calculated from the optical density measured at 535 nm with a Hitachi U-2800 spectrophotometer. A_{535} was measured after incubation in the dark at 22–25 °C with 250 rpm shaking in an assay solution that contained 5 mM MES buffer (pH 5.5), 300 μM (BPDS), and 100 μM iron(III)-EDTA unless stated otherwise. Pea embryos were dissected with a surgical blade as fast as possible and kept in 5 mM MES buffer (pH 5.5) for 30 min, representing the time to dissect and weigh around 15 embryos. Embryos were then incubated in the assay solution.

To measure root ferric chelate reductase activity, whole root systems from individual pea plants were excised, rinsed three times with demineralized water, and incubated in 50 ml of assay solution following the same protocol. The comparison of embryo ferric chelate reductase activities was repeated five times independently, and each experiment consisted of the incubation of five embryos in 5 ml of assay solution with the usual protocol. Final results are the mean ± S.D. of the five values obtained. *Arabidopsis* root ferric chelate reductase activity was measured from individual root systems of iron-deficient seedlings in 1 ml of assay solution.

Ferric Reduction Activity Measurement of Exudates—Exudates consisted of 5 ml Milli-Q water in which five pea embryos were incubated, representing a total fresh weight of 0.7–1 g. For the efflux kinetics, embryos were incubated 10, 20, and 30 min or immersed and removed immediately for the 0-min time point. 100 μM iron(III)-EDTA and 300 μM BPDS were then added to exudates and allowed to react for 1 h in the dark prior to A_{535} determination. For the comparison of exudate activity with embryo activity, exudates were collected in Milli-Q water after 30 min of incubation and allowed to react with 100 μM iron(III)-EDTA and 300 μM BPDS for 1 h in the dark. In the case of ascorbate oxidase (AOX) treatment, 1.5 unit of AOX/ml of exudate was added 2 min before iron(III)-EDTA and BPDS addition. In this experiment, embryo ferrireduction activity was quantified following 30 min of embryo incubation in Milli-Q water containing 100 μM iron(III)-EDTA and 300 μM BPDS and 1 h incubation in the dark without embryos. All final values are the mean ± S.D. of three independent experiments.

Time Course of Embryo Fe Reduction—In this experiment, individual embryos were incubated in 2 ml of assay solution containing 0, 0.15, or 1.5 AOX units/ml. A_{535} was determined after 0, 10, 20, 30, 40, and 50 min of incubation from 2.5 μl of solution using a Nanodrop 1000 (Thermo Scientific). The experiment was carried out with five individual embryos per treatment and repeated three times. Values are the mean of the three experiments ± S.D.

^{55}Fe Accumulation in Pea Embryos—Embryos weighting 20–50 mg were isolated and weighed as fast as possible after pod harvesting. They were individually disposed in 24-well plates containing 2 ml of the following solution: 100 mM KCl, 5 mM $CaSO_4$, and 5 mM MES (pH 5.5). Influx was initiated by replacing this solution with influx buffer, which consisted of the same solution supplemented with 100 μM iron(III)-EDTA and

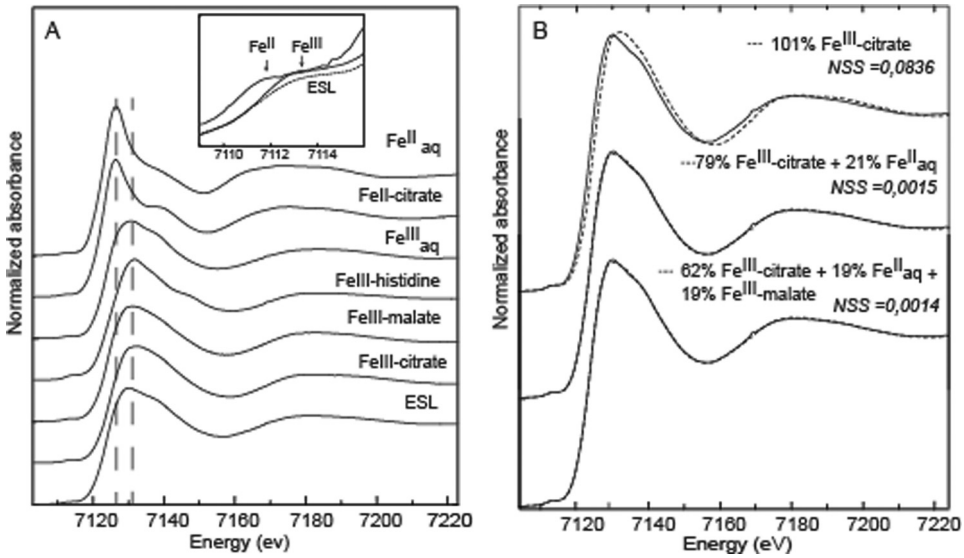

FIGURE 1. **Iron(III) predominates in the ESL.** Iron K-edge XANES spectra of ESL and selected iron model compounds (*A*) with the pre-edge structures of iron(II)$_{aq}$, iron(III)$_{aq}$, and ESL (*inset*). *B*, one-, two-, and three-component fits (*dotted lines*) of the ESL XANES spectrum (*solid lines*). The quality of the fit was evaluated by the normalized sum-squares residuals, $NSS = \Sigma i(Xanes_{experimental} - Xanes_{fit})^2 / \Sigma i(Xanes_{experimental}) \times 100$.

0.2 μCi/ml ^{55}Fe. In the BPDS- and AOX-treated samples, 4 mM BPDS or 1.5 AOX units/ml were also provided in the uptake buffer. Embryos were incubated for 40 min in the dark at either 30 or 4 °C. The reaction was stopped by rinsing embryos three times with an ice-cold solution containing 1 mM KCl, 10 mM EDTA, 1 mM $FeCl_3$, 10 mM $CaCl_2$, 5 mM $MgSO_4$, and 5 mM MES (pH = 5.5).

^{55}Fe was quantified following PerkinElmer Life Sciences instructions. Embryos were transferred to glass vials and dried for 48 h at 50 °C. They were then dissolved in 100 μl of perchloric acid at 50 °C for 24 h. Sample were cleared by adding 200 μl of hydrogen peroxide and incubated at 50 °C until complete bleaching. 3 ml of HionicFluor scintillating mixture (PerkinElmer Life Sciences) was added to the samples. Counts per minute were measured with a Tri-carb liquid scintillation counter (PerkinElmer Life Sciences) and converted to degradations per minute by QuantaSmart software (PerkinElmer Life Sciences) using the tSIE/AEC quenching correction. The iron quantity was deduced from the activity of a standard vial containing 10 μl of uptake buffer and 3 ml of HionicFluor. Net influx values were obtained by subtracting the quantity of ^{55}Fe accumulated at 4 °C. The final Fe accumulation corresponds to the mean ± S.E. (n = 3) of data obtained with 12 individual embryos from three independent experiments.

RESULTS

Iron Speciation in The Embryo Sac Liquid by XANES—The aim of the XANES spectroscopy measurements was to examine the redox status of iron and the potential iron complexes in the ESL under conditions minimizing the possible changes of iron species during sample preparation and analyses. For that, the ESL sample was frozen immediately after collection and analyzed without any chemical additive and in the frozen state to limit speciation change and beam radiation damage.

XANES spectra of iron references show that the edge of iron(II) compounds is shifted to lower values compared with iron(III) compounds, as expected (Fig. 1*A*). Iron complexes involving malate and citrate, where the metal is coordinated by oxygen atoms from carboxyl groups, show similar spectral features but can be distinguished from iron-histidine.

The ESL spectrum edge mainly exhibits edge features of iron(III) compounds (Fig. 1*A*). However, the spectrum did not match one iron species only, and results of linear combination fitting showed that a mixture of 79% iron(III)-citrate and 21% iron(II)$_{aq}$ gave a satisfactory fit (NSS = 0.0015, Fig. 1*B*). A correct match is also obtained for a combination of iron(III)-citrate and iron(II)-citrate (data not shown, NSS = 0.0020), suggesting the presence of a minor iron(II) species, that was not clearly identified. Fits with iron(III)-malate instead of iron(III)-citrate gave a poorer agreement (NSS = 0.0022), and the improvement of the simulation, when considered as a third component, was not significant (NSS = 0.0014). We can thus infer that the major part of iron is present as iron(III) in the ESL, probably as organic acids, whereas a minor iron(II) species can occur but remains unidentified. Although it is difficult to clearly rule out a possible photoreduction under beam exposure (29), this effect was checked by successive collection of spectra on the samples. No reduction was observed, neither on the ESL nor on the iron(III) model compounds, and, thus, we can infer that the occurrence of iron(II) is not an artifact.

Iron Speciation in the Embryo Sac Liquid—The analysis of iron speciation in the embryo sac liquid was performed by alternatively coupling hydrophilic liquid chromatography to two different mass spectrometry instruments, an ICP MS to determine the number of significant iron-containing species within this sample and quantify iron and an ESI MS to identify the corresponding species (retention time matching) using the same chromatographic conditions. HILIC chromatography has been established recently as an adequate technique to preserve and separate metal complexes originating from raw samples, allowing their identification and quantification by mass spectrometry (18). It was applied here to the liquid endosperm samples. Prior to analyses, iron recovery was tested during sample

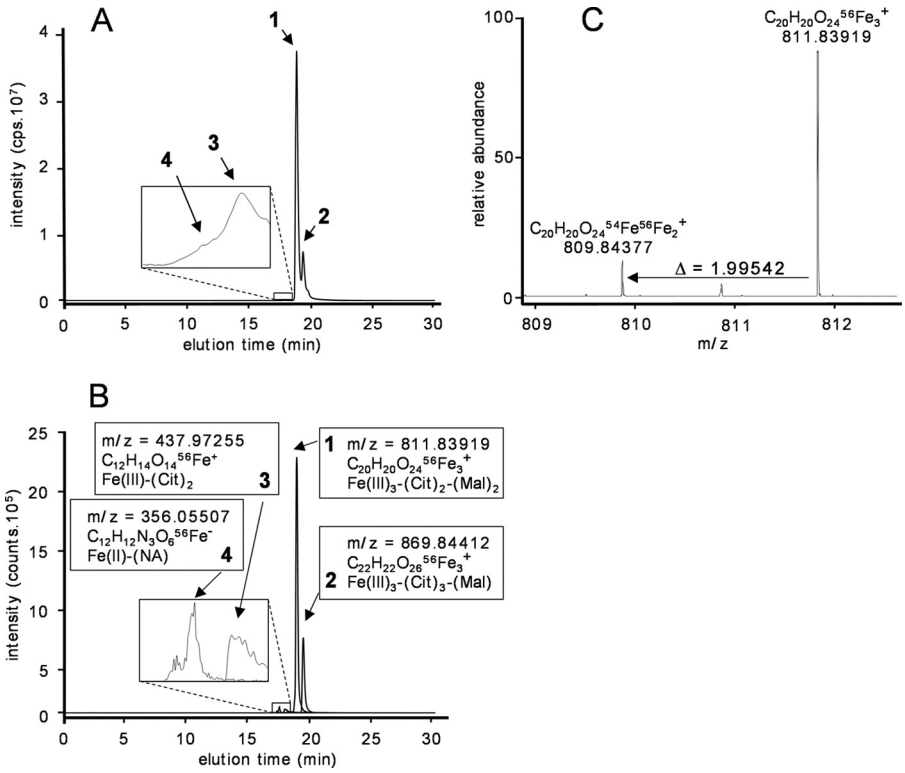

FIGURE 2. **Molecular identification of the ligands in the iron-containing complexes.** Analysis of iron speciation in liquid endosperm by HILIC ICP MS following ^{56}Fe (*A*) and HILIC ESI MS, in positive mode for compounds 1–3, following compound 1 at *m/z* 811.84, compound 2 at *m/z* 869.85, compound 3 at *m/z* 437.97, and compound 4 at *m/z* 356.05507 in negative mode (*B*). *C*, an example of zoomed mass spectrum obtained for compound 1 eluting at 18.8 min with its specific isotopic profile because of the contribution of the two main iron isotopes, ^{54}Fe and ^{56}Fe. *cps,* counts/s.

preparation (mixing with acetonitrile followed by centrifugation) and during the chromatographic run. An overall 85 ± 8% of iron species were conserved after the two consecutive procedures, which meant that significant amounts of the original iron species were conserved by this method. After chromatographic coupling with ICP MS, two major iron species as well as a minor iron species were detected (Fig. 2*A*). By HILIC ESI MS in positive ion mode, these iron-containing compounds were identified, respectively, as compound 1 at m/z 811.84, compound 2 at m/z 869.85, and compound 3 at *m/z* 437.97 (Fig. 2*B*). MS^2 fragmentation of compounds 1 and 2 allowed to determine that organic molecules containing exclusively carbon, hydrogen, and oxygen with carboxylic acid groups were surrounding a nucleus constituted of three ions of iron, which was consistent with the observed isotopic profile (Fig. 2*C*). It was deduced that these two metal complexes were constituted of a mixture of citrate (Cit) and malate (Mal) binding three iron(III) ions. Each of these two complexes then contains four organic acid molecules, two citrate molecules, and two malate molecules in compound 1 ($Fe(III)_3Cit_2Mal_2$) and three citrate molecules and one malate molecule for compound 2 ($Fe(III)_3Cit_3Mal_1$). Compound 3 was found to be a complex between two citrate molecules and one iron(III) ion ($Fe(III)Cit_2$). According to this, the chemical formula of each complex could be determined, and experimental and theoretical masses could be compared: compound 1, $C_{20}H_{20}O_{24}Fe_3^+$, m/z_{exp} 811.83919, m/z_{theo} 811.83873, δm = 0.6 ppm; compound 2, $C_{22}H_{22}O_{26}Fe_3^+$, m/z_{exp} 869.84412, m/z_{theo} 869.84421, $\delta m = -0.1$ ppm; and compound 3, $C_{12}H_{14}O_{14}Fe^+$, m/z_{exp} 437.97255, m/z_{theo} 437.97275, $\delta m = -0.5$ ppm. The analysis of a standard mixture of iron(III)-citrate-malate (0.2:1:5 ratio, buffered at pH 5.5 with ammonium acetate) definitively confirmed the formation of these iron-citrate-malate complexes through the appearance of the above-mentioned *m/z* (compounds 1 and 2) in MS spectra. The mixed complex structures is unclear, but is probably similar to the $iron(III)_3Cit_3$ complex structure as postulated by Fukushima *et al.* (17). That is, a Fe_3 core is expected to occur with iron ions bound to each other through α-hydroxy groups of organic acids, and carboxylic groups are surrounding iron ions. The absence of an Fe_3Cit_3 complex in the analyzed sample seems to indicate that the mixed iron(III)-citrate-malate would be an even more stable species.

Traces of an iron(II)-NA complex (compound 4, $C_{12}H_{18}N_3O_6Fe^-$, m/z_{exp} 356.05507, m/z_{theo} 356.05506, δm = 0.0 ppm) were also detected in negative ion mode (Fig. 2*B*), even when oxic (because of sampling and chromatography) and acidic (pH 5.5) conditions were not favorable to the presence of this form compared with iron(III)-organic acid complexes. Even when iron(III) was the preponderant iron form in the sample, iron(III)-NA could not be detected, which seemed to indicate that NA would have a relative higher affinity for iron(II) than for iron(III) in the presence of citrate and malate, suggesting a differentiated speciation depending on the iron redox status.

Pea Embryos Are Capable of Ferric Reduction through Ascorbate Efflux—Strategy I plants are not able to perform direct transport of ferric iron, but, instead, rely on a ferric reduction step prior to ferrous ion uptake. Therefore, we wondered

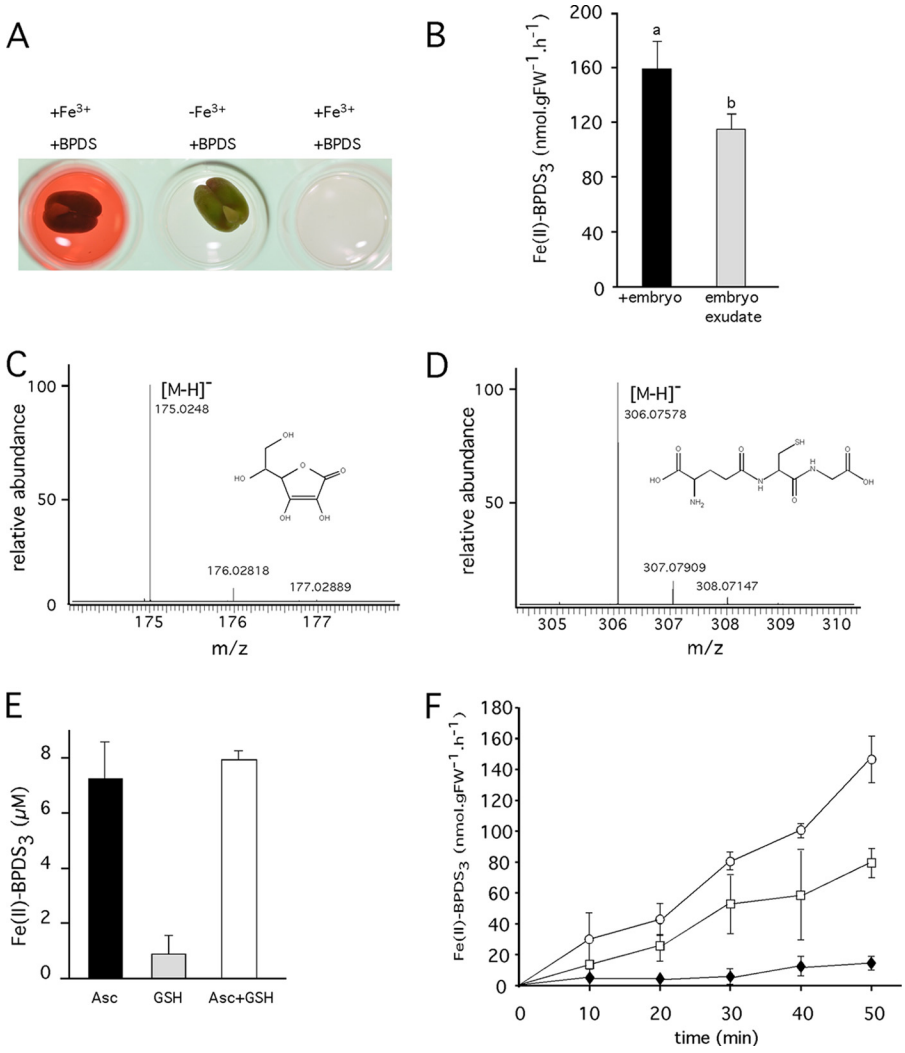

FIGURE 3. **The ferric reduction activity of pea embryos is mediated by ascorbate efflux.** *A*, isolated embryos were incubated for 2 h in a 5 mM MES buffer (pH 5.5) with 100 μM iron(III)-EDTA and 300 μM BPDS (*left well*) and in a control medium without iron(III)-EDTA (*center well*). In the *right well*, a complete assay medium without embryos was incubated under the same conditions. *B*, ferric reduction activity measured by the BPDS method in the presence of embryos (+*embryo*) or after removing the embryos (*embryo exudate*). Results are the mean ± S.D of three independent replicates. Different *letters* indicate significant differences among the means ($p < 0.05$ by Tukey's test). *C* and *D*, electrospray ionization mass spectrometry analysis of reducing compounds effluxed by embryos showing the presence of ascorbate (*C*) and glutathione (*D*) in the efflux medium. *E*, *in vitro* reduction of ferric iron by ascorbic acid (*Asc*) and glutathione. 100 μM iron(III)-EDTA and 300 μM BPDS were incubated with 5 μM ascorbic acid or 5 μM glutathione or both. $A_{535\ nm}$ was measured 30 min after addition of reductants. Results are the mean ± S.D. of two replicates. *F*, ferric reduction activity of pea embryos incubated in 5 mM MES (pH 5.5) with 100 μM iron(III)-EDTA and 300 μM BPDS without AOX (○) or in the presence of 0.15 and 1.5 AOX units/ml (□ and ◆, respectively). The absorbance at 535 nm was measured every 10 min. Each curve was built from the mean ± S.D. of three independent experiments that consisted in measuring the activities of five individual embryos for each treatment.

whether ferric chelate reduction was also part of the iron uptake machinery of the embryo. Embryonic ferric chelate reductase activity was assayed by incubating isolated immature pea embryos with the Fe^{2+} chelator BPDS in the presence or the absence of Fe^{3+}. With Fe^{3+} in the assay, the embryos were capable of generating Fe^{2+}, visualized by the formation of a pink iron(II)-$BPDS_3$ complex (Fig. 3*A*). In contrast, no coloration was detected when Fe^{3+} was omitted in the incubation medium (Fig. 3*A*, $-Fe^{3+} + BPDS$), thereby ruling out the possibility that production of an iron(II)-$BPDS_3$ complex is caused by the secretion of Fe^{2+} by the embryo. Therefore, we concluded that pea embryos are capable of reducing exogenous Fe^{3+}.

To check whether the ferric reduction activity was catalyzed by a FRO-like transmembrane reductase or mediated by the efflux of reductive compounds, we compared the ferric reduction activity measured with embryos in the medium to the activity of embryo exudates (*i.e.* by removing the embryos before measuring iron reduction). Surprisingly, the reduction activity measured after removing the embryos was almost as high as the one obtained with embryos in the medium (Fig. 3*B*). This result indicates that, contrary to what has been described in roots, most of the reduction activity of pea embryos is due to the efflux of potent reductants in the medium.

Because the most obvious candidates reducing molecules in plants are ascorbic acid and glutathione, we looked whether these compounds were present in embryo exudates by ESI MS. As expected, ascorbate and glutathione could be detected by ESI MS analysis of embryo exudates (Fig. 3, *C* and *D*). To discriminate between these two molecules, we tested their capac-

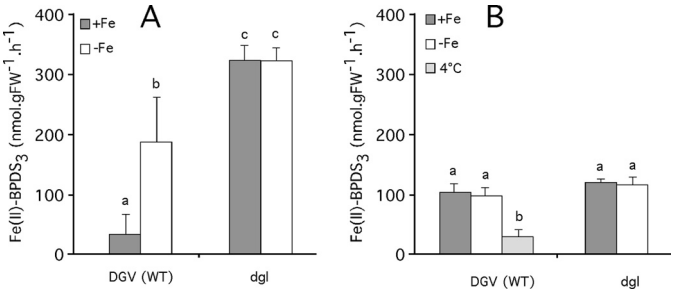

FIGURE 4. **The embryo ferric chelate reduction is not regulated by the iron nutritional status.** *A*, root ferric chelate reductase activity was measured on excised roots of individual wild-type (*DGV*) or mutant (*dgl*) plants by incubation for 15 min in 100 ml of 5 mM MES buffer (pH 5.5) with 100 μM iron(III)-EDTA and 300 μM BPDS. *B*, embryo ferric reduction activity was carried out with five embryos incubated for 15 min in 5 ml of 5 mM MES buffer (pH 5.5) with 100 μM iron(III)-EDTA 300 μM FerroZine. Each experiments was repeated three times, and results are the mean of the three replicates ± S.D. Significant differences (indicated by the different *letters*) were determined with a parametric Tukey test ($p < 0.05$).

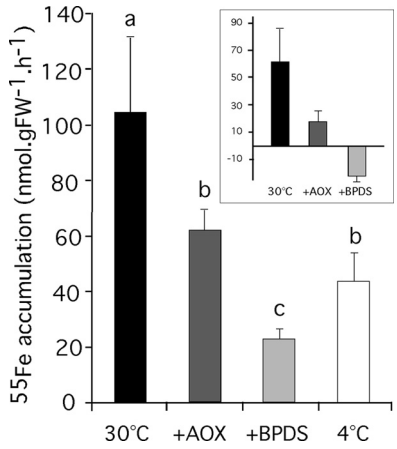

FIGURE 5. **Ascorbate-mediated ferric reduction is an obligatory step for iron influx.** ^{55}Fe influx was measured in isolated pea embryos. Embryos were incubated in uptake buffer containing 100 μM iron(III)-EDTA, and, when stated, 4 mM BPDS or 1.5 AOX units/ml (+*AOX*) was added. Incubation at 4 °C with the complete uptake medium was also realized to measure passive adsorption of iron at the embryo surface. *Inset*, net influx of ^{55}Fe deduced by calculating the difference between iron accumulation at 30 °C (complete, +*AOX*, +*BPDS*) and the 4 °C control incubation. Each measurement was performed on four to five embryos of 20–50 mg, and experiments were repeated three times independently. Results are the mean ± S.E. ($n = 3$). Significant differences (indicated by the different *letters*) were determined with a nonparametric Kruskal-Wallis test ($p < 0.05$).

ity to reduce ferric iron *in vitro* under the conditions used with embryos (100 μM Fe^{3+}, 300 μM BPDS). Under these conditions, we could show that ascorbate, but not glutathione, was necessary and sufficient to spontaneously reduce iron *in vitro* (Fig. 3*E*). To confirm that the iron-reducing molecule effluxed by embryos was ascorbate, we tested the effect of AOX on the reducing activity of isolated embryos over 50 min of incubation. The time course analysis of iron reduction, linear for 50 min, was strongly inhibited by AOX in a dose-dependent manner (Fig. 3*F*), confirming that ascorbic acid secreted by the embryos was responsible for the ferric reduction activity measured with isolated embryos.

We then checked whether this reduction activity was regulated by the iron status, as described previously for the root reductase. Pea plants were thus grown in hydroponic culture under standard (50 μM iron) or deficiency conditions (no iron added). As expected, the root reductase activity was strongly induced under iron deficiency conditions (Fig. 4*A*). However, the reduction activity of embryos isolated from +iron and −iron plants was not significantly different (Fig. 4*B*). We also used the iron signaling mutant *dgl* that constitutively expresses the iron acquisition machinery in roots (30). Consistent with previous reports, the root reductase activity was constitutively high, regardless of the iron status (Fig. 4*A*), although the reduction activity of embryos was not significantly different, neither between +iron and −iron nor between the wild-type (DGV) and the mutant embryos (*B*). In conclusion, contrary to the root system, the ferric reduction activity expressed at the embryo surface is not regulated by the iron status.

Pea Embryos Take up Ferrous Iron—To assess the importance of ascorbate-mediated ferric reduction for embryo iron uptake, we quantified the accumulation of the radioactive isotope ^{55}Fe, provided as iron(III)-EDTA, into isolated embryos. To evaluate Fe^{2+} and Fe^{3+} uptake rates by the embryo, an uptake assay was set up by adding either AOX, to prevent the formation of Fe^{2+} because of ascorbate-mediated reduction, or BPDS, which is expected to scavenge newly formed Fe^{2+}. The rationale for this experiment was that if an ascorbate-mediated reduction step is required, then both BPDS and AOX should inhibit the uptake.

Untreated embryos accumulated 105 (±27) nmol/g of fresh weight/h when incubated at 30 °C and 43 (±11) nmol/g FW/h at 4 °C. In the presence of AOX and BPDS, the iron accumulation rates, not significantly different from the 4 °C control, were, respectively, 62 (±8) and 22 (±4) nmol/g FW/h (Fig. 5). When expressed as net influx, by subtracting the iron accumulation at 4 °C, it appeared clearly that both BPDS and AOX significantly inhibited the uptake of iron by isolated embryos (Fig. 5, *inset*). On the basis of these results, it was concluded that ascorbate-mediated ferric reduction is an absolute requirement for iron uptake by pea embryos, thus uncovering a new role for ascorbate in plants.

Ascorbate Efflux Is Not Limited to the Pea—These new findings on pea embryos prompted us to check whether this ascorbate efflux activity was a general mechanism, found in other species such as the model plant *A. thaliana*. Embryos were isolated (bent cotyledon stage) from developing siliques of *Arabidopsis* (Fig. 6*A*, *inset*), and iron reduction activity was measured as described previously for peas (Fig. 3). *Arabidopsis* embryos were indeed capable of reducing iron, and this activity was reduced significantly by the addition of AOX in the incubation medium (Fig. 6*A*). This ferric reduction activity appeared to be fully attributable to ascorbate efflux because the rates obtained with embryos or with exudates (*i.e.* after removal of embryos from the medium) were not significantly different. The addition of AOX to embryo exudates completely abolished iron reduction, confirming the identity of ascorbic acid as the main reductant effluxed by *Arabidopsis* embryos (Fig. 6*A*). As a control for AOX specificity on the ascorbate-mediated reduction, we checked the effect of AOX on the well established root ferric reductase activity mediated by the membrane protein FRO2. We thus assayed the reductase activity of *Arabidopsis* roots isolated from iron-sufficient and iron-deficient plants (Fig. 6*B*). As shown previously, iron-deficient roots exhibited higher fer-

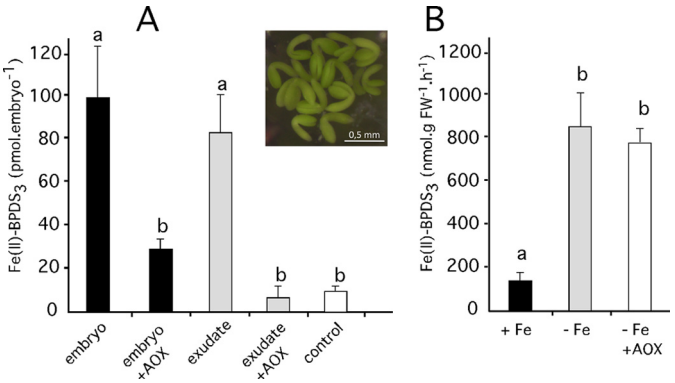

FIGURE 6. **The ascorbate efflux mechanism is conserved in *A. thaliana* embryos.** *A*, embryos at the bent torpedo stage were dissected and incubated to measure the ferric reduction activity, either with embryos in the medium or after removing the embryos to measure the activity on the exudates. When stated, AOX was added to the incubation medium. Results are the mean ± S.D. of three independent replicates. Each condition in an individual experiment was realized with 30–50 embryos. Different letters indicate significant differences among means ($p < 0.05$ by Tukey's test). *B*, the root ferric chelate reductase activity is not inhibited by AOX. Ten-day-old seedlings grown in 50 μM iron(III)-EDTA (*+Fe*) were transferred in a medium without iron and supplemented with 30 μM FerroZine (*-Fe*) for 3 days and then assayed for ferric reductase activity. When stated, AOX was added to the incubation medium. Values are the mean of five plants, and different letters indicate significant differences among means ($p < 0.05$ by Tukey's test).

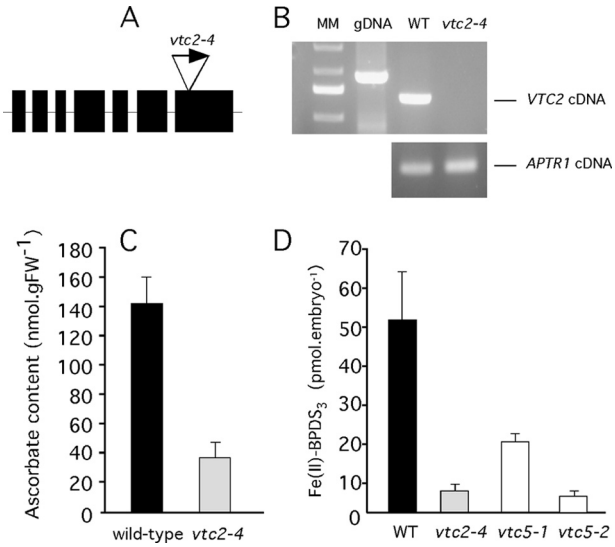

FIGURE 7. **Ascorbate synthesis-deficient mutants have reduced embryo reduction activity.** *A–C*, isolation and characterization of the *vtc2-4* knockout allele (SALK_146824). *A*, position and orientation of the T-DNA in the last exon of the *VTC2* coding region. *B*, *VTC2* expression analysis by RT-PCR on wild-type plants and the *vtc2-4* mutant. *MM*, molecular weight markers; *gDNA*, genomic DNA. Equal loading of cDNA from the WT and *vtc2-4* was verified by amplification of the *APTR1* (proline-rich extensin-like family protein, At1g27450) cDNA. Primers used to amplify VCT2 cDNA were as follows: 5′-ATGTTGAAAATCAAAAGAGTTCCGACCGTTG-3′ and 5′-TCACTGAAGGACAAGGCACTCGGC-3′. Primers for APTR1 were as follows: 5′-CGCTTCTTCTCGACACTGAG-3′ and 5′-CAGGTAGCTTCTTGGGTTC-3′. *C*, ascorbate concentration (reduced form) in leaves of the wild type and the *vtc2-4* mutant. Results are the mean ± S.D. of three independent replicates. *D*, ferric reduction activity of isolated embryos. Embryos were dissected (bent cotyledon stage) and incubated to measure the ferric reduction activity. Results are the mean ± S.D of three independent replicates. Each condition in an individual experiment was realized with 30–50 embryos.

ric chelate reductase activity than iron-replete roots (Fig. 6*B*). Interestingly, this activity was not significantly inhibited by AOX, indicating that ferric reduction in roots is biochemically different from that in embryos.

Finally, we sought to make a genetic link between iron reduction and accumulation with ascorbate metabolism. We thus analyzed the reduction activity and iron concentration in seeds and embryos on several vitamin C-defective (VTC) mutants, affected in ascorbate synthesis (31). We first isolated a new T-DNA insertion line of the *VTC2* gene, *vtc2-4* (Fig. 7*A*) and showed, by RT-PCR, that it was a knockout allele (Fig. 7*B*). This mutation led to a 70% decrease in ascorbate accumulation in leaves (Fig. 7*C*), which is in agreement with previous results on other *vtc2* alleles (31). Embryos were then isolated from *vtc2-4*, *vtc5-1*, and *vtc5-2* mutant seeds to measure ferric reduction activity.

Compared with the wild type, the iron reduction activity of the *vtc* mutant embryos was reduced significantly (Fig. 7*D*). Furthermore, the iron accumulation in mature embryos of *vtc2-4*, *vtc5-1*, and *vtc5-2* was also significantly lower than in the wild type, as shown by Perls staining that reveals iron by a blue coloration (Fig. 8*A*). Wild-type mature embryos contained detectable amounts of iron in the veins, whereas, in *vtc5* embryos, the staining was very faint, and *vtc2-4* embryos did not contain detectable amounts of iron (Fig. 8*A*). The total iron content in whole dry seeds was also significantly lower in *vtc* mutants compared with the wild type (Fig. 8*B*). Collectively, these data demonstrate that embryos acquire iron through a new strategy of iron reduction and uptake that is dependent on, and mediated by, ascorbate synthesis and efflux.

DISCUSSION

In this work, we studied the mechanism of iron entry into the seed through two approaches: an iron speciation analysis at the interphase between the seed coat and embryo in the pea, associated with a biochemical dissection of iron transport on isolated embryos of the pea and *Arabidopsis*. We established that iron is delivered by the maternal tissues as ferric complexes with citrate and malate, that the embryos are capable of reducing the ferric ions of these complexes through the efflux of ascorbate, and that this reducing activity is an obligatory step for iron transport as iron(II). The analysis of iron speciation is by far the least documented aspect of iron homeostasis, both in animals and plants. This is principally due to the difficulties of obtaining biologically reliable samples (*i.e.* without mixing cellular compartments and creating artifact complexes) and the low concentration of iron in living tissues. To our knowledge, the iron speciation analysis reported in this study is one of the few unambiguous reports on the identification of iron complexes *in vivo*. Ferric-citrate complexes have long been proposed to occur in apoplastic compartments, but only recently a has a speciation approach led to the molecular identification of a tri-iron(III) tricitrate complex as the major iron-circulating form in the xylem of tomato plants (9). The ESL of pea seeds, although highly concentrated in nutrients (sugars, amino acids, etc.) from symplastic origin (32), is characterized by an acidic pH (5.4) that is similar to the pH of an apoplastic compartment. Thus, our findings reinforce previous *in silico* (12) and *in vitro* studies (13) that demonstrated that, under mildly acidic conditions, ferric citrate would be the most stable and abundant type of complex, despite the presence of other ligands like nicotianamine. Moreover, our data identified malate as a new player in

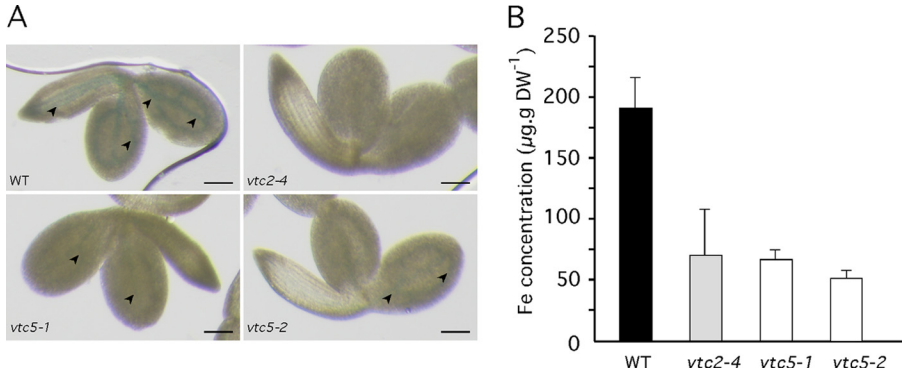

FIGURE 8. **Ascorbate synthesis-deficient mutants accumulate less iron in embryos and whole seeds.** *A*, mature embryos were dissected from dry seeds and stained for iron with Perls reagent. Positive staining of iron is revealed by a blue coloration in the provascular system (*arrowheads*). *Scale bars* = 0.15 mm. *B*, seeds of WT, *vtc2-4*, *vtc5-1*, and *vtc5-2* mutant plants were collected, and iron was quantified. Results are the mean ± S.D. of three independent replicates.

iron speciation in plants. Although one of the metabolic responses to iron deficiency is the accumulation of organic acids, including malate (34), a direct role of malic acid has never been clearly established. Instead, malate has been involved in the hyperaccumulation of nickel in *T. caerulescens* leaf extract (18) and *Alyssum serpyllifolium* with the formation of complexes with nickel in the xylem sap (35). Malate was also found to be involved in the storage of zinc in the leaves of the hyperaccumulator *Arabidopsis halleri* (36). Malate is also a key molecule for the tolerance to aluminium because it is excreted from roots by aluminium-activated malate transporters to chelate aluminium in the rhizosphere (37–39). Aluminium-activated malate transporter family members, therefore, represent putative candidate transporters whose function could be to load malate in the embryo sac liquid. Belonging to the same multidrug and toxic compound extrusion family of transporters as aluminium-activated malate transporters, FRD3 is a citrate efflux transporter that has been proposed recently to play a critical role in the movement of iron between tissues that are not symplastically connected. A detailed analysis of the expression pattern of FRD3 and a phenotypical analysis of *frd3* knockout mutants have demonstrated the importance of FRD3-mediated citrate efflux in iron unloading in the leaf (from the xylem to adjacent cells) and in the anther (from the tapetum to pollen grains) (10). Interestingly, the seed coat and the embryo protodermis are also disconnected completely, and FRD3 is highly expressed in both tissues in *A. thaliana* (10). Thus, citrate efflux by FRD3 could be important as well to load the ESL with citrate and, subsequently, induce the formation of iron-citrate complexes. More generally, our results strengthen the importance of citrate in the transport of iron between cells and organs. Citrate may, in fact, be a ubiquitous and important intercellular iron ligand. Indeed, in mammals citrate is the main ligand of the non-transferrin-bound iron species (40, 41), which appear to be the most abundant chemical form of iron circulating in the extracellular medium of the brain (42, 43), used as a source of iron for brain cells (44). Most of the iron present in the liquid endosperm was found to be Fe^{3+} bound to a mixture of citrate and malate. It is the first observation *in vivo* of such mixed complexes. Compounds 1 and 2 correspond to two iron complexes that most likely participate in binding iron(III) to form a soluble, stable (contrary to the iron(III)Cit_2 complex, for example), but low-reactive species. Indeed, iron(III) alone would precipitate, leading to iron deficiency, whereas its presence in a weakly complexed form would probably lead to increased stress for the plant because of expected frequent random exchanges of the Fe^{3+} ion with other nonspecific binding sites in surrounding molecules. Therefore, these mixed complexes with organic acids probably participate in making iron(III) available in the liquid endosperm for transport/reaction, such as reduction by ascorbate in the vicinity of the embryo, without inducing significant metal or oxidative stress.

The identification of iron(II)-nicotianamine in the ESL represents the definitive proof of the *in vivo* role of nicotianamine in the movement of iron, although, in our case, the proportion of this complex is several orders of magnitude lower than the iron bound to organic acids. Nevertheless, the presence of iron-NA in the ESL could be interpreted as the signature of the activity of YSL transporters. The fact that iron translocation to the seed is controlled, in part, by YSL transporter activity has been shown in *Arabidopsis*. The closely related members AtYSL1 and AtYSL3 have been involved in the loading of iron, zinc, and copper to the seeds (20, 21). In particular, the mutation in *AtYSL1*, which is expressed in the chalazal endosperm of the seed, provokes a reduced accumulation of iron and NA in mature seeds (20). Thus, the presence of iron-NA complexes, the *bona fide* substrate of YSL transporters, in the ESL leads to the assumption that iron is delivered from the seed coat to the ESL by YSL proteins.

Up to now, there has been no direct functional link between the metabolism of ascorbate and iron homeostasis. Instead, several reports had described the induction of ascorbate accumulation in response to iron deficiency and proposed that it could represent a mechanism to cope with potential reactive oxygen species production (45, 46). The most unexpected finding of this study was the discovery of ascorbate efflux as the mechanism to reduce and acquire iron from the ferric complexes. Although other organic molecules, such as phenolics, can be excreted by roots of strategy I plants in response to iron deficiency, these molecules are not capable of reducing iron(III) in the medium (47). Furthermore, the iron reduction activity has, so far, only been attributed to membrane proteins of the FRO family, such as the plasma membrane proteins FRO2, FRO4, and FRO5 (2, 48) and the chloroplastic protein FRO7 (49). In

contrast, this report describes a new strategy of iron acquisition on the basis of a reduction activity that is independent of the FRO proteins but, instead, relies on the property of ascorbate as a powerful reductant. Unlike the root ferric reductase activity, the ascorbate-mediated reduction was not induced by iron deficiency or in the *dgl* mutant that constitutively expresses the iron deficiency responses, irrespective of the iron nutritional status, strengthening the idea that this new mechanism is molecularly distinct from the FRO-based iron transport and not regulated by the iron deficiency signaling pathway. Furthermore, we have shown that the ascorbate efflux activity is also expressed in *A. thaliana* embryos. To further confirm the link between ascorbate metabolism and iron acquisition, we used mutants affected in ascorbate synthesis. The *VTC2* and *VTC5* genes encode two isoforms of GDP-L-galactose phosphorylase, one of the last enzymes of the ascorbate biosynthetic pathway (31, 50). In terms of expression, *VTC2* is predominant, and disruption of this gene provokes a 70% decrease in ascorbate accumulation in leaves, whereas mutations in *VTC5* barely affect ascorbate accumulation (31). Both genes are expressed in *A. thaliana* embryos, and we show here that both mutations greatly impact the ascorbate efflux, iron accumulation in seeds and mature embryos. These data confirm the biochemical characterization performed in pea embryos and establish a direct and genetic link between ascorbate metabolism and iron transport in the plant.

Interestingly, a comparable iron uptake mechanism has been proposed in mammals. Erythroleukemia K562 cells and astrocytes are capable of reducing iron(III) using ascorbate efflux, generating iron(II) and dehydroascorbate that is reabsorbed to regenerate an ascorbate pool in the cytosol (51, 52). Transmembrane cycling of ascorbate coupled to ferrous transport by the divalent transporter DMT1 appears as one possible route for iron accumulation in these cell types. Yet, in contrast to the constitutively high ascorbate efflux activity measured in embryos, ascorbate efflux was only triggered when cells were supplied with elevated dehydroascorbate levels. The molecular identity of the efflux transport system remains unknown in both plants and mammals, but the biochemical features of ascorbate efflux in mammalian K562 cells were compatible with the activity of an anion channel (51). Ascorbate efflux by pea embryos was insensitive to anion channel inhibitors (data not shown) but required a pH gradient, suggesting that it could be mediated by an H^+/ascorbate antiporter. The importance of the proton motive force has already been reported for the transport of nutrients in pea embryos on the basis of the specific expression in the outer cell layer of the cotyledons of genes encoding H^+/sucrose and H^+/amino acid cotransporters (33, 53). Future work will be aimed at molecularly identifying this ascorbate efflux system.

Acknowledgments—We thank the Soleil Synchrotron (Gif sur Yvette, France) for the provision of beamtime (Project 20110430) and Nicolas Trcera from the LUCIA Beamline for help and advice during data collection. We also thank Nicholas Smirnoff for discussions regarding the vtc mutants.

REFERENCES

1. Santi, S., and Schmidt, W. (2009) Dissecting iron deficiency-induced proton extrusion in Arabidopsis roots. *New Phytol.* **183,** 1072–1084
2. Robinson, N. J., Procter, C. M., Connolly, E. L., and Guerinot, M. L. (1999) A ferric-chelate reductase for iron uptake from soils. *Nature* **397,** 694–697
3. Eide, D., Broderius, M., Fett, J., and Guerinot, M. L. (1996) A novel iron-regulated metal transporter from plants identified by functional expression in yeast. *Proc. Natl. Acad. Sci. U.S.A.* **93,** 5624–5628
4. Henriques, R., Jásik, J., Klein, M., Martinoia, E., Feller, U., Schell, J., Pais, M. S., and Koncz, C. (2002) Knock-out of *Arabidopsis* metal transporter gene IRT1 results in iron deficiency accompanied by cell differentiation defects. *Plant Mol. Biol.* **50,** 587–597
5. Varotto, C., Maiwald, D., Pesaresi, P., Jahns, P., Salamini, F., and Leister, D. (2002) The metal ion transporter IRT1 is necessary for iron homeostasis and efficient photosynthesis in *Arabidopsis thaliana*. *Plant J.* **31,** 589–599
6. Vert, G., Grotz, N., Dédaldéchamp, F., Gaymard, F., Guerinot, M. L., Briat, J. F., and Curie, C. (2002) IRT1, an *Arabidopsis* Transporter essential for iron uptake from the soil and for plant growth. *Plant Cell* **14,** 1223–1233
7. Green, L. S., and Rogers, E. E. (2004) FRD3 controls iron localization in *Arabidopsis*. *Plant Physiol.* **136,** 2523–2531
8. Durrett, T. P., Gassmann, W., and Rogers, E. E. (2007) The FRD3-mediated efflux of citrate into the root vasculature is necessary for efficient iron translocation. *Plant Physiol.* **144,** 197–205
9. Rellán-Alvarez, R., Giner-Martínez-Sierra, J., Orduna, J., Orera, I., Rodríguez-Castrillón, J. A., García-Alonso, J. I., Abadía, J., and Alvarez-Fernández, A. (2010) Identification of a tri-iron(III), tri-citrate complex in the xylem sap of iron-deficient tomato resupplied with iron. New insights into plant iron long-distance transport. *Plant Cell Physiol.* **51,** 91–102
10. Roschzttardtz, H., Séguéla-Arnaud, M., Briat, J. F., Vert, G., and Curie, C. (2011) The FRD3 citrate effluxer promotes iron nutrition between symplastically disconnected tissues throughout *Arabidopsis* development. *Plant Cell* **23,** 2725–2737
11. Stacey, M. G., Patel, A., McClain, W. E., Mathieu, M., Remley, M., Rogers, E. E., Gassmann, W., Blevins, D. G., and Stacey, G. (2008) The *Arabidopsis* AtOPT3 protein functions in metal homeostasis and movement of iron to developing seeds. *Plant Physiol.* **146,** 589–601
12. von Wiren, N., Klair, S., Bansal, S., Briat, J. F., Khodr, H., Shioiri, T., Leigh, R. A., and Hider, R. C. (1999) Nicotianamine chelates both Fe^{III} and Fe^{II}. Implications for metal transport in plants. *Plant Physiol.* **119,** 1107–1114
13. Rellán-Alvarez, R., Abadía, J., and Alvarez-Fernández, A. (2008) Formation of metal-nicotianamine complexes as affected by pH, ligand exchange with citrate and metal exchange. A study by electrospray ionization time-of-flight mass spectrometry. *Rapid Commun. Mass Spectrom.* **22,** 1553–1562
14. Pich, A., and Scholz, G. (1996) Translocation of copper and other micronutrients in tomato plants (*Lycopersicon esculentum* Mill). Nicotianamine-stimulated copper transport in the xylem. *J. Exp. Bot.* **47,** 41–47
15. Mari, S., Gendre, D., Pianelli, K., Ouerdane, L., Lobinski, R., Briat, J. F., Lebrun, M., and Czernic, P. (2006) Root-to-shoot long-distance circulation of nicotianamine and nicotianamine-nickel chelates in the metal hyperaccumulator *Thlaspi caerulescens*. *J. Exp. Bot.* **57,** 4111–4122
16. Trampczynska, A., Küpper, H., Meyer-Klaucke, W., Schmidt, H., and Clemens, S. (2010) Nicotianamine forms complexes with Zn(II) *in vivo*. *Metallomics* **2,** 57–66
17. Fukushima, T., Sia, A. K., Allred, B. E., Nichiporuk, R., Zhou, Z., Andersen, U. N., and Raymond, K. N. (2012) *Bacillus cereus* iron uptake protein fishes out an unstable ferric citrate trimer. *Proc. Natl. Acad. Sci. U.S.A.* **109,** 16829–16834
18. Ouerdane, L., Mari, S., Czernic, P., Lebrun, M., and Lobinski, R. (2006) Speciation of non-covalent nickel species in plant tissue extracts by electrospray Q-TOF MS/MS after their isolation by 2D size-exclusion-hydrophilic interaction LC (SEC-HILIC) monitored by ICP MS. *J. Anal. At. Spectrom.* **21,** 676–683
19. Klatte, M., Schuler, M., Wirtz, M., Fink-Straube, C., Hell, R., and Bauer, P. (2009) The analysis of *Arabidopsis* nicotianamine synthase mutants reveals functions for nicotianamine in seed iron loading and iron deficiency

responses. *Plant Physiol.* **150,** 257–271
20. Le Jean, M., Schikora, A., Mari, S., Briat, J. F., and Curie, C. (2005) A loss-of-function mutation in AtYSL1 reveals its role in iron and nicotianamine seed loading. *Plant J.* **44,** 769–782
21. Waters, B. M., Chu, H. H., Didonato, R. J., Roberts, L. A., Eisley, R. B., Lahner, B., Salt, D. E., and Walker, E. L. (2006) Mutations in *Arabidopsis* yellow stripe-like1 and yellow stripe-like3 reveal their roles in metal ion homeostasis and loading of metal ions in seeds. *Plant Physiol.* **141,** 1446–1458
22. Walker, E. L., and Waters, B. M. (2011) The role of transition metal homeostasis in plant seed development. *Curr. Opin. Plant Biol.* **14,** 318–324
23. Patrick, J. W. (1997) Phloem unloading. Sieve element unloading and post-sieve element transport. *Annu. Rev. Plant Physiol. Plant Mol. Biol.* **48,** 191–222
24. Patrick, J. W., and Offler, C. E. (2001) Compartmentation of transport and transfer events in developing seeds. *J. Exp. Bot.* **52,** 551–564
25. Van Dongen, J. T., Ammerlaan, A. M., Wouterlood, M., Van Aelst, A. C., and Borstlap, A. C. (2003) Structure of the developing pea seed coat and the post-phloem transport pathway of nutrients. *Ann. Bot.* **91,** 729–737
26. Flank, A. M., Cauchon, G., Lagarde, P., Bac, S., Janousch, M., Wetter, R., Dubuisson, J. M., Idir, M., Langlois, F., Moreno, T., and Vantelon, D. (2006) LUCIA, a microfocus soft XAS beamline. *Nucl. Instrum. Methods Phys. Res. B* **246,** 269–274
27. Wilke, M., Farges, F., Petit, P. E., Brown, G. E., and Martin, F. (2001) Oxidation state and coordination of Fe in minerals. An FeK-XANES spectroscopic study. *Am. Mineral.* **86,** 714–730
28. Gustafsson, J. P. (2006) *Visual MINTEQ*, version 2. 51, KTH, Royal Institute of Technology, Stockholm, Sweden
29. Terzano, R., Mimmo, T., Vekemans, B., Vincze, L., Falkenberg, G., Tomasi, N., Schnell Ramos, M., Pinton, R., and Cesco, S. (2013) Iron (Fe) speciation in xylem sap by XANES at a high brilliant synchrotron X-ray source: opportunities and limitations. *Anal. Bioanal. Chem.* **405,** 5411–5419
30. Grusak, M. A., and Pezeshgi, S. (1996) Shoot-to-root signal transmission regulates root Fe(III) reductase activity in the dgl mutant of pea. *Plant Physiol.* **110,** 329–334
31. Dowdle, J., Ishikawa, T., Gatzek, S., Rolinski, S., and Smirnoff, N. (2007) Two genes in *Arabidopsis thaliana* encoding GDP-L-galactose phosphorylase are required for ascorbate biosynthesis and seedling viability. *Plant J.* **52,** 673–689
32. Melkus, G., Rolletschek, H., Radchuk, R., Fuchs, J., Rutten, T., Wobus, U., Altmann, T., Jakob, P., and Borisjuk, L. (2009) The metabolic role of the legume endosperm. A noninvasive imaging study. *Plant Physiol.* **151,** 1139–1154
33. Tegeder, M., Offler, C. E., Frommer, W. B., and Patrick, J. W. (2000) Amino acid transporters are localized to transfer cells of developing pea seeds. *Plant Physiol.* **122,** 319–326
34. López-Millán, A. F., Morales, F., Abadía, A., and Abadía, J. (2001) Iron deficiency-associated changes in the composition of the leaf apoplastic fluid from field-grown pear (*Pyrus communis* L.) trees. *J. Exp. Bot.* **52,** 1489–1498
35. Alves, S., Nabais, C., Simões Gonçalves Mde, L., and Correia Dos Santos, M. M. (2011) Nickel speciation in the xylem sap of the hyperaccumulator *Alyssum serpyllifolium* ssp. *lusitanicum* growing on serpentine soils of northeast Portugal. *J. Plant Physiol.* **168,** 1715–1722
36. Sarret, G., Willems, G., Isaure, M. P., Marcus, M. A., Fakra, S. C., Frérot, H., Pairis, S., Geoffroy, N., Manceau, A., and Saumitou-Laprade, P. (2009) Zinc distribution and speciation in *Arabidopsis halleri* × *Arabidopsis lyrata* progenies presenting various zinc accumulation capacities. *New Phytol.* **184,** 581–595
37. Delhaize, E., Ryan, P. R., Hebb, D. M., Yamamoto, Y., Sasaki, T., and Matsumoto, H. (2004) Engineering high-level aluminum tolerance in barley with the ALMT1 gene. *Proc. Natl. Acad. Sci. U.S.A.* **101,** 15249–15254
38. Sasaki, T., Yamamoto, Y., Ezaki, B., Katsuhara, M., Ahn, S. J., Ryan, P. R., Delhaize, E., and Matsumoto, H. (2004) A wheat gene encoding an aluminum-activated malate transporter. *Plant J.* **37,** 645–653
39. Hoekenga, O. A., Maron, L. G., Piñeros, M. A., Cançado, G. M., Shaff, J., Kobayashi, Y., Ryan, P. R., Dong, B., Delhaize, E., Sasaki, T., Matsumoto, H., Yamamoto, Y., Koyama, H., and Kochian, L. V. (2006) AtALMT1, which encodes a malate transporter, is identified as one of several genes critical for aluminum tolerance in *Arabidopsis*. *Proc. Natl. Acad. Sci. U.S.A.* **103,** 9738–9743
40. Evans, R. W., Rafique, R., Zarea, A., Rapisarda, C., Cammack, R., Evans, P. J., Porter, J. B., and Hider, R. C. (2008) Nature of non-transferrin-bound iron. Studies on iron citrate complexes and thalassemic sera. *J. Biol. Inorg. Chem.* **13,** 57–74
41. Hider, R. C., Silva, A. M. N., Podinovskaia, M., and Ma, Y. M. (2010) in *Cooley's Anemia. Ninth Symposium* (Vichinsky, E. P., and Neufeld, E. J. eds), pp. 94–99, New York Academy of Science, New York
42. Bradbury, M. W. (1997) Transport of iron in the blood-brain-cerebrospinal fluid system. *J. Neurochem.* **69,** 443–454
43. Moos, T., Rosengren Nielsen, T., Skjørringe, T., and Morgan, E. H. (2007) Iron trafficking inside the brain. *J. Neurochem.* **103,** 1730–1740
44. Bishop, G. M., Dang, T. N., Dringen, R., and Robinson, S. R. (2011) Accumulation of non-transferrin-bound iron by neurons, astrocytes, and microglia. *Neurotox. Res.* **19,** 443–451
45. Zaharieva, T. B., and Abadía, J. (2003) Iron deficiency enhances the levels of ascorbate, glutathione, and related enzymes in sugar beet roots. *Protoplasma* **221,** 269–275
46. Urzica, E. I., Casero, D., Yamasaki, H., Hsieh, S. I., Adler, L. N., Karpowicz, S. J., Blaby-Haas, C. E., Clarke, S. G., Loo, J. A., Pellegrini, M., and Merchant, S. S. (2012) Systems and trans-system level analysis identifies conserved iron deficiency responses in the plant lineage. *Plant Cell* **24,** 3921–3948
47. Jin, C. W., You, G. Y., He, Y. F., Tang, C., Wu, P., and Zheng, S. J. (2007) Iron deficiency-induced secretion of phenolics facilitates the reutilization of root apoplastic iron in red clover. *Plant Physiol.* **144,** 278–285
48. Bernal, M., Casero, D., Singh, V., Wilson, G. T., Grande, A., Yang, H., Dodani, S. C., Pellegrini, M., Huijser, P., Connolly, E. L., Merchant, S. S., and Krämer, U. (2012) Transcriptome sequencing identifies SPL7-regulated copper acquisition genes FRO4/FRO5 and the copper dependence of iron homeostasis in *Arabidopsis*. *Plant Cell* **24,** 738–761
49. Jeong, J., Cohu, C., Kerkeb, L., Pilon, M., Connolly, E. L., and Guerinot, M. L. (2008) Chloroplast Fe(III) chelate reductase activity is essential for seedling viability under iron limiting conditions. *Proc. Natl. Acad. Sci. U.S.A.* **105,** 10619–10624
50. Laing, W. A., Wright, M. A., Cooney, J., and Bulley, S. M. (2007) The missing step of the L-galactose pathway of ascorbate biosynthesis in plants, an L-galactose guanyltransferase, increases leaf ascorbate content. *Proc. Natl. Acad. Sci. U.S.A.* **104,** 9534–9539
51. Lane, D. J., and Lawen, A. (2008) Non-transferrin iron reduction and uptake are regulated by transmembrane ascorbate cycling in K562 cells. *J. Biol. Chem.* **283,** 12701–12708
52. Lane, D. J., Robinson, S. R., Czerwinska, H., Bishop, G. M., and Lawen, A. (2010) Two routes of iron accumulation in astrocytes. Ascorbate-dependent ferrous iron uptake via the divalent metal transporter (DMT1) plus an independent route for ferric iron. *Biochem. J.* **432,** 123–132
53. Tegeder, M., Wang, X. D., Frommer, W. B., Offler, C. E., and Patrick, J. W. (1999) Sucrose transport into developing seeds of *Pisum sativum* L. *Plant J.* **18,** 151–161

Ascorbate Efflux as a New Strategy for Iron Reduction and Transport in Plants

Louis Grillet, Laurent Ouerdane, Paulina Flis, Minh Thi Thanh Hoang, Marie-Pierre Isaure, Ryszard Lobinski, Catherine Curie and Stéphane Mari

J. Biol. Chem. 2014, 289:2515-2525.
doi: 10.1074/jbc.M113.514828 originally published online December 17, 2013
